



Are ghost forests a substantial source of methane from reservoirs?

Johannes Dittmann¹, Damien T. Maher¹, Scott G. Johnston¹, Douglas R. Tait¹, Paula Gomez Alvarez¹, Alistair Grinham², Katrin Sturm³, and Luke C. Jeffrey¹

JFaculty of Science and Engineering, Southern Cross University, Lismore, NSW, 2480, Australia Faculty of Engineering, Architecture and Information Technology, St Lucia, The University of Queensland, QLD, Australia

³Seqwater, 117 Brisbane Street, Ipswich QLD 4305, Australia

Correspondence to: Johannes Dittmann (j.dittmann.10@student.scu.edu.au)

10 Abstract. Methane (CH₄) is a potent greenhouse gas that is increasing in the atmosphere, being a major driver of climate change. Tree stem CH4 emissions are a rapidly advancing research field however emissions from dead trees remain poorly studied. This is of particular concern in reservoir "ghost forests", where large areas of standing dead trees can form, and remain submerged in CH₄-enriched waters, providing a potential CH₄-flux pathway along the soil-tree-atmosphere continuum, for many decades. This study quantified the drivers of seasonal CH₄ and 15 carbon dioxide (CO₂) emissions from a ghost forest within a subtropical reservoir alongside diffusive and ebullition fluxes, across two seasons. We compared the influence of sediment organic carbon, water level and temperature fluctuations on ghost forest stem CH₄ emissions, to the diffusive and ebullition flux pathways, at three within reservoir sites (North, Mid and South). The highest average ghost forest CH₄ fluxes occurred near the reservoir inflow site (South) during summer (1173 ± 338 µmol m⁻² stem d⁻¹). At the same location the average 20 CH₄ fluxes from ghost forest trees and ebullition were significantly higher, 5.8 and 2.7 respectfully, during summer, compared to winter. Ghost forest CH₄ fluxes contributed an additional ~15% to the overall reservoir greenhouse gas budget, beyond conventional methods which generally only consider ebullition and diffusive flux pathways. Our findings reveal the need to recognise ghost forest CH₄ emissions from reservoirs and encourage management strategies to balance CH₄ mitigation with other ecological benefits of standing ghost forests.

25 1. Introduction

30

Methane (CH₄) and carbon dioxide (CO₂) concentration in the atmosphere have been increasing rapidly since the industrial revolution (Saunois et al., 2020; Friedlingstein et al., 2020), contributing to increased radiative forcing driving climate change. CH₄ has a warming potential ~28 times higher than CO₂ over a 100-year time scale (Boucher et al., 2009) accounting for about one third of the rise in global temperatures. Within the global CH₄ budget, freshwaters and inland waters are identified as major sources of CH₄ (Saunois et al., 2020). Overall, inland waters globally emit between 197 to 396 Tg of CH₄ per year, with approximately half originating from wetlands and roughly a third by lakes and reservoirs (Rosentreter et al., 2021). However, large uncertainty still exists around CH₄ emissions related to these systems (Rosentreter et al., 2024; Saunois et al., 2020; Saunois et al., 2025).

Within freshwater ecosystems, CH₄ is primarily produced in anaerobic sediments by methanogenesis (Rudd and Hamilton, 1978). Methanogens are influenced by different environmental factors that enhance or limit CH₄ production, including temperature, organic substrate, nutrients, and oxygen supply (Megonigal et al., 2003). CH₄

https://doi.org/10.5194/egusphere-2025-5594 Preprint. Discussion started: 19 November 2025 © Author(s) 2025. CC BY 4.0 License.





produced within anaerobic sediments can be emitted to the atmosphere via ebullition and diffusive pathways. However, vegetation-mediated CH₄ fluxes have gained recognition as an important CH₄ flux pathway in freshwater wetlands (Bastviken et al., 2022; Vroom et al., 2022). During the growing season, herbaceous plant-mediated fluxes can be the major source of CH₄ in some wetlands (e.g., (Jeffrey et al., 2019a; Whiting and Chanton, 1992; Carmichael et al., 2014). More recently, wetland tree stems have also been shown to act as an active conduit for soil-produced CH₄ and the atmosphere (Barba et al., 2024; Barba et al., 2019). Dead forests or ghost forests, can also emit CH₄ via their stems (Carmichael et al., 2018; Carmichael and Smith, 2016).

45

50

40

The formation of ghost forests can occur naturally during dieback events, natural disasters, sea level rise, mismanagement or through the effects of climate change (Carmichael and Smith, 2016; Smart et al., 2020). They can also form after flooding of catchments during reservoir and dam construction (Romero-Uribe et al., 2022). The number of dam and reservoirs for hydro-power is expected to double by the end of this decade (Zarfl et al., 2015). Within reservoirs, ghost forests provide a unique situation as standing dead trees provide a passive soil-CH₄ gas-transport conduit, due to the hollowing out of the tree internal cavities and hydraulic system after forest mortality, while the saturated timber substrate also supports carbon degradation and CH₄ production by fungal and methanogenic microbes (Carmichael et al., 2018; Jeffrey et al., 2019b). Though the precise drivers and sources of CH₄ are complex.

55

60

65

70

75

Coastal ghost forests, caused by water table rise and seawater inundation, were found to emit CH₄ primarily originating from the soil (Martinez et al., 2022). In the same study, only ~10 % of anaerobic wood core incubations showed evidence for CH₄ production, suggesting that CH₄-produced by wood decomposition processes were less important than soil derived CH₄. Furthermore, methanogen communities were detected in only ~20% of ghost forest wood samples of the same location, with 10% of wood incubations producing CH₄ (Carmichael et al., 2024). In dead trees, internal CH₄ production by microbial and fungal wood decay have been suggested as a more important source of CH₄ (Covey and Megonigal, 2018). This is especially important in the years following tree mortality (Covey et al., 2016) as fungal and microbial community composition shift, during the decomposition stages, as different forms of carbon become available (Hu et al., 2017). Therefore, ghost forest stem CH₄ emissions may be modulated by a combination of soil CH₄ transportation, *in situ* methanogenesis, and/or microbial CH₄ oxidation.

Ghost forest tree stems can be a significant CH₄ source, exceeding the rates of living trees. For instance, dead mangrove forests were shown to emit eight times more CH₄ than nearby living mangroves (Jeffrey et al., 2019b). Similarly, dead cypress trees in Japan had higher CH₄ emissions than living trees (Sakabe et al., 2025). Furthermore, CH₄ emissions from dead woody debris in temperate forests (Covey et al., 2016; Kipping et al., 2022) and tropical forests (Kumar et al., 2021) suggests that CH₄ emissions from dead trees may be an overlooked process in all forest types. Overall research on ghost forest tree stem CH₄ emissions is currently limited, with the majority of research conducted in North America (Carmichael et al., 2018; Martinez et al., 2022; Martinez and Ardón, 2021).





Although it is recognized that ghost forests tree stems emit CH₄ and CO₂, to the best of our knowledge, no study has determined the significance of ghost forest CH₄ emissions within a reservoir CH₄ budget. Here, we addressed that question, and compared them to conventionally studied aquatic and ebullition CH₄ flux pathways. We assessed the significance of these fluxes across three different site locations, and between two distinct seasons to estimate the importance of this previously unquantified CH₄ source.

2. Methodology

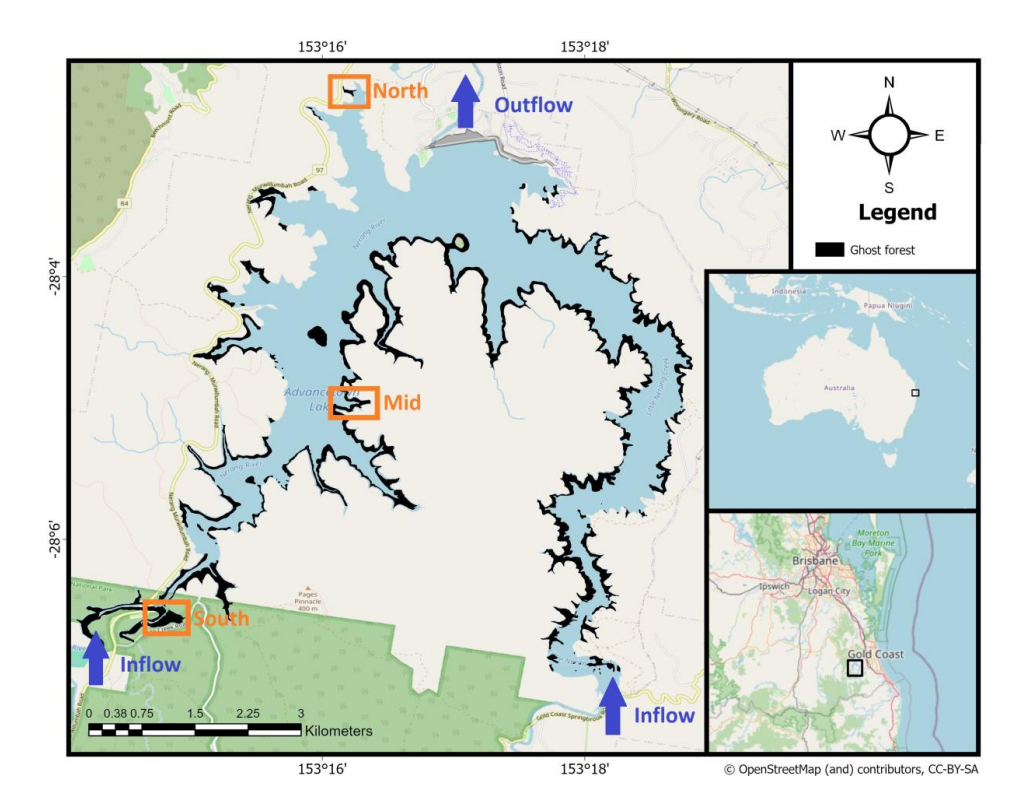
80

85

90

2.1 Study site

The study took place at Hinze Dam (28.05056°S, 153.28389°E) located near Gold Coast, Australia (Fig. 1). The reservoir was built across the Nerang River in 1976, creating a large artificial lake with a maximum supply volume of 310,730 megalitres. The reservoir provides drinking water to the Gold Coast population (~650,000) and helps to mitigate floods. The reservoir wall height was raised in 1989, then again in 2011, increasing the water level by 15 meters and doubling its capacity. The increase in water level in 2011 led to the death of trees around the lake perimeter, now covering ~20 % of the reservoir surface area, creating the existing ghost forest. The western part of the reservoir is connected to the Nerang River and Waterfall Creek, while the eastern part is connected to Little Nerang Creek, with the Little Nerang Dam upstream. There is a small dam that reduces the amount of fresh organic material coming into the eastern side of the lake.





105

110



Figure 1: Map of Hinze Dam, showing the extent of the ghost forest (black) covering approximately 20% of the reservoir surface area. The three study sites (North, Mid, and South) are marked in orange.

2.2 Field campaigns

Two field campaigns were conducted in the winter (mid-August) and early summer (late November) of 2023 to capture seasonal variability in temperature and water level. All sampling was conducted from boats to minimize benthic disturbances within each plot. The three plots were located to the South, Mid and North of the reservoir western arm, which accounts for an inflow depositional gradient from South to North (Fig. 1). In the South, the Nerang River stream feeds the reservoir and deposits sediment and organic material which has been shown to result in higher CH₄ ebullition hotspots in the southern inlets (Sherman and Ford, 2011). Trees were sampled in belt transects perpendicular to the shoreline (Fig. 2a-c), which allowed us to measure trees along a water depth gradient. All trees sampled were in standing water during both field campaigns (Fig. 2d). The same trees were resampled in both seasons, keeping the stem height above the water surface consistent between campaigns, as the water table dropped.

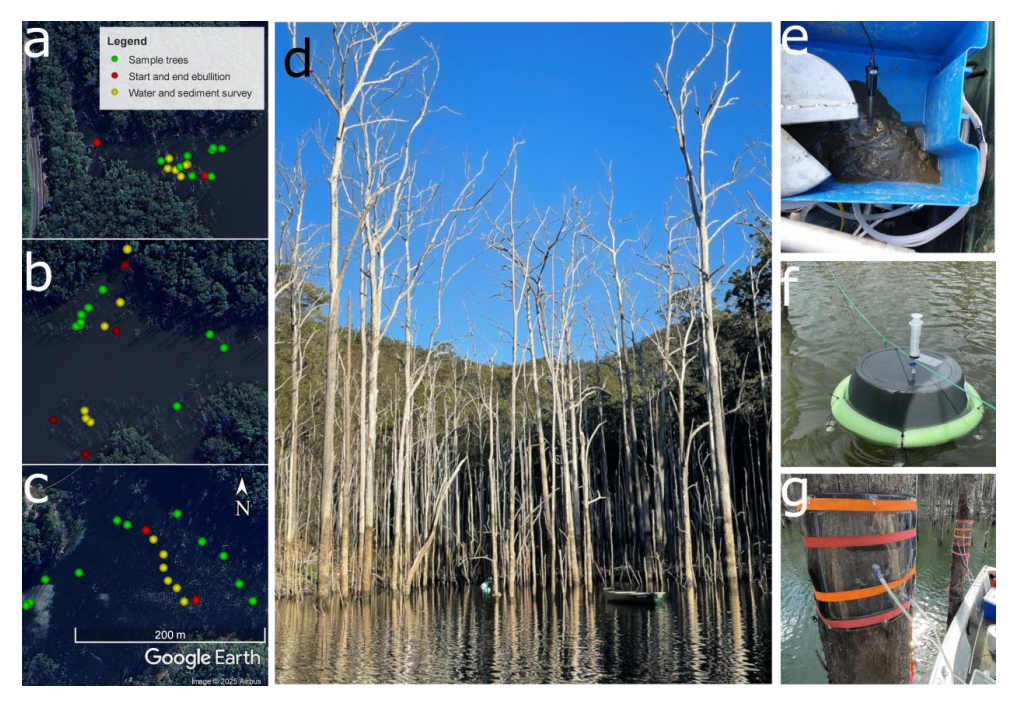


Figure 2: Layout of the three study plots in Hinze Dam during the summer campaign, showing the North (a), Mid (b), and South (c) sites. The panels show the sample trees, the start and end points of the ebullition transects, and the sediment and water survey sampling locations. Further panels show: A ghost forest embayment (d), sediment sampling (e), an ebullition chamber (f), and a tree chamber (g).





2.3 Sediment sampling

A Van Veen grab was used to collect benthic sediments from six locations per site (Fig. 2e). The pH and redox potential of the sediments were measured *in situ* using a pre-calibrated multiprobe (Hach PHC101 and MTC301). During the first campaign, three soil samples were also taken at each site and analysed for total nitrogen, phosphorus, δ¹³C (‰) and % C_{org} with samples oven dried at 40°C and then homogenised before analysis. Total nitrogen was determined using a LECO TruMac CNS analyser. Phosphorus samples were first treated with a 1:3
 Nitric/HCl and then run on APHA 3125 ICPMS. Carbon content samples were pre-treated with acid to remove inorganic carbon before analyses on an Elemental Analyser (EA). During the second campaign, the depth of the organic-rich layer was estimated by gently tapping a 10 cm Ø PVC pipe through the softer sediments until the hard clay layer was reached, and measuring the depth change. This was replicated at three locations per site. The sediment oxygen demand (SOD) was determined by adding 10 g of freshly collected sediment (Van Veen grab) into a 250 mL borosilicate glass bottle, filling it with surface water and noting the start and stop concentrations of dissolved oxygen at 0 and 48 hours (Hach, LDO101).

2.4 Aquatic CH₄ concentrations

130

135

140

145

150

To determine aquatic CH₄ concentrations, 150 ml water samples were collected into borosilicate bottles at six locations within each site along a water depth gradient. Surface (10 cm) and bottom water samples (30 cm above the benthic surface) were collected using a peristaltic pump, overflowing > 3 times the bottle volume before capping ensuring no headspace. The samples were initially kept on ice until later being treated with mercury (II) chloride (HgCl₂) at the end of the sampling day. Water temperature and dissolved oxygen levels were also measured at the same locations using a hand-held probe (Hach, LDO101). Additionally, a spatial transect collecting water samples (as described above) at ~1 km intervals along the reservoir was performed on each trip, spanning from the southern to northern plot (Winter n=16 and summer n=23 locations). The coordinates, windspeed and water depth were also noted at each sample location. The dissolved partial pressure of pCH₄ and pCO₂ and δ ¹³C values were determined using the headspace method with a 90 mL water sample and 60 mL of ambient air added into a 150ml syringe and shaken vigorously for 2 min (Jeffrey et al., 2019a). The headspace gas was then analysed using a CO₂/CH₄ isotope cavity ringdown spectrometer (Picarro CRDS, G2201-i) and then corrected for the dilution with ambient air.

2.5 Ebullition fluxes

To quantify ebullition at each site, ten floating bubble traps were established along a perpendicular transect from the shoreline within the ghost forest (n=30) (Fig. 2a-c & f). Gas within the headspace of each chamber was collected every -24 hours. Each chamber had a 30 mL syringe pre-attached to the chamber outlet, which was extracted carefully to minimize disturbance to the chamber. The 30 mL gas sample was then transferred into duplicate evacuated 12 mL exetainer vials. The gas samples were later analysed for CH₄ and CO₂ concentrations using the CRDS and a small sample induction module (Picarro SSIM, A0314).

2.6 Tree stem and aquatic CH₄ fluxes

The ghost forest tree stem CO₂ and CH₄ fluxes were measured by attaching semi-rigid foam-lined airtight chambers onto the tree stems (Siegenthaler et al., 2016) (Fig. 2g). Each tree stem CO₂ and CH₄ flux was measured





160

165

at three different heights between 10 cm and 220 cm above the water level) to account for variability of fluxes along stem height (Pangala et al., 2013). Chambers that were attached above algae, bark or over cracks were noted (Fig. S1). To prevent potential chamber leaks due to small cracks, fissures or rough bark surfaces, white plotting clay was applied to seal these areas (Jeffrey et al., 2020b). Individual gas fluxes were measured for three to seven minutes, with longer measurements required for lower fluxing tree stem surfaces. Diffusive aquatic CH₄ fluxes were measured adjacent to ghost forest trees by placing a 28 cm diameter circular floating chamber onto the water surface. The tree stem and aquatic flux chambers were connected to a portable cavity ring-down spectrometer CO₂ and CH₄ analyser (CRDS Picarro, G4301) and CO₂ and CH₄ flux rates were measured *in situ*. The CRDS precision was factory calibrated ±0.3 ppb with a lower detection limit of 0.9 ppb. The stem circumference and flux chamber height above the water level were noted for each sample tree, along with the water depth.

2.7 Ghost forest tree stem internal gas concentrations

Ghost forest internal tree stem gas concentrations were collected from 11 trees spread across each site similar to Carmichael and Smith (2016). Multiple 12 cm deep (13 mm internal diameter) holes were drilled horizontally into each tree stem at lower stem heights, using a cordless electric drill, with the hole immediately sealed using a sterilized rubber septum stopper. Gases were allowed to accumulate in the stem cavity for 24 hours, at which time ~12 ml of stem gas were removed and injected into a pre-evacuated exetainer, with the precise volume of gas sample noted. The CH₄ concentration was determined using the CRDS SSIM (as described above).

2.8 Flux calculations and upscaling

The stem and aquatic CH₄ and CO₂ flux (s) rates were processed using a modified gas flux R script "GasFlux"

(Version 0.6-1). The results of the linear regression for each flux measurement (Fig. S2) were added into the following Eq. 1:

$$F = \left(s\left(\frac{V}{RT_{air}A}\right)\right)t \tag{Eq. 1}$$

where s is the regression slope in ppm sec⁻¹ for each flux measurement, V is the chamber volume (m³) (which includes the CRDS volume, chamber and tubing volume), R is the universal gas constant (8.205 × 10⁻⁵ m³.atm $^{-1}$.K $^{-1}$.mol $^{-1}$), T_{air} is the mean air temperature of the chamber in the CRDS (°K), A is the chamber surface area (m²) and t is the conversion factor from seconds to day, and to μ mol of CO₂/CH₄. Linear regression of CO₂/CH₄ fluxes of t were used in the calculation. Linear regression of t values were used as a proxy for assessing air-tight chamber seals, especially in lower CH₄ fluxing trees.

180

185

175

The ebullition CH_4 flux rates E were calculated according to Eq. 2:

$$E = \left(\left(\frac{CH_{4 end} - CH_{4 start}}{T_d} \right) * \left(\frac{V}{RT_{air}A} \right) * t \right) - F_w$$
 Eq. 2

where T_d is the duration of the deployment time, CH_{4end} is final headspace concentration (ppm), CH_{4start} is assumed 1.9 ppm and F_w is the average aquatic diffusive CH_4 flux at each site (as determined in Eq. 1). The dissolved CO_2 and CH_4 concentrations from water samples were calculated using the head space equilibration method according to Eq. 3:



195

200

205

210

215

220



$$GHG_{\text{w sample}} = \frac{GHG_p}{V_w} \left(KV_w + \frac{1}{RT} V_V \right)$$
 Eq. 3

where V_w is the volume of the water used, V_v the volume of the headspace, GHG_p is the CO_2/CH_4 concentration (ppmV) measured with the SSIM CRDS. To upscale the axial tree stem CO_2/CH_4 fluxes to individual tree emissions, the diameter at breast height (DBH in cm) was used to estimate the diameter of each tree and assumes trees were cylinders with no branching. To conservatively estimate total stem gas fluxes, we only up-scaled up to a height of 2.5 meters above the water level (i.e., trees were in excess of 30 m in height). The cylindric form was divided into three radial bands and calculated as follows (Eq. 4):

$$F_t = \int_0^{2.5} (c * h * F)$$
 Eq. 4

where F_t is the flux per tree up to 2.5 m (µmol day⁻¹), c is the tree circumference calculated with the DBH in (m), F is the *in situ* measured gas flux rate for that height (µmol m⁻² d⁻¹) and h is the height of each band (m). The height per band was the same as the height of the chamber plus half the distance to the next chamber, or the distance to either end of 2.5 m. The density of trees (trees ha⁻¹) of the ghost forest was estimated from duplicate 100 m² plots in the Northern site and four 100 m² plots in the South and Mid sites. Tree heights were measured during May 2025 using a laser range finder (Nikon, Forestry Pro). The overall ecosystem CH₄ flux from trees for each site was calculated using Eq. 5:

$$F_{tol} = xF_t * d * c$$
 Eq. 5

where F_{tol} is the total tree flux per ha (mol d⁻¹), xF_t is the mean flux per tree, d is the tree density (trees ha⁻¹) and c is the conversion factor from μ mol d⁻¹ to mol d⁻¹. To upscale the aquatic and ebullition flux inside the ghost forest area, the sum of the tree basal surface areas was subtracted from the total aquatic surface area. The remaining aquatic surface area was multiplied by the average areal aquatic and ebullition CH₄ flux rates per site. To compare the different pathways for reservoir CH₄ emissions, first the total emission from tree stems were estimated by determining the average CH₄ emissions from tree stems on an areal basis, using tree density from within each 100 m² plots and the average tree CH₄ emissions per site. The total basal area of the trees from within each ghost forest site were deducted from the average areal CH₄ flux rate for ebullition and diffusive CH₄ fluxes (Note: tree basal areas only accounted for 1.6 ± 0.4 , 1.6 ± 0.5 and 2.5 ± 1.0 % of the ghost forested area within South, Mid and North sites, respectively).

The total surface area of the reservoir, the ghost forested areas and the shallow zones around the edges (8 m water depth) were estimated using ArcGIS Pro (version 3.4.0), using a bathymetry map provided by Seqwater. Ebullition was assumed to only occur in all areas < 8 m in depth (Bastviken et al., 2004). For the open water areas of the reservoir (not containing trees), the diffusive CH₄ flux was estimated using spatially collected dissolved CH₄ concentrations (from the transect grab samples above) and the CH₄ flux rate numerically modelled using *k* estimated from windspeed (Wannikhof, 1992). We separated the reservoir surface area into three zones, the southern zone (with the inflow), the middle zone (spanning most of the open water reservoir including the eastern part) and the northern zone (which combines the far north and eastern embayment). The average flux per site for each of the three CH₄ pathways (trees, aquatic and ebullition) for each trip was used in the calculation. The sum of the three pathways represents the total zone emissions.





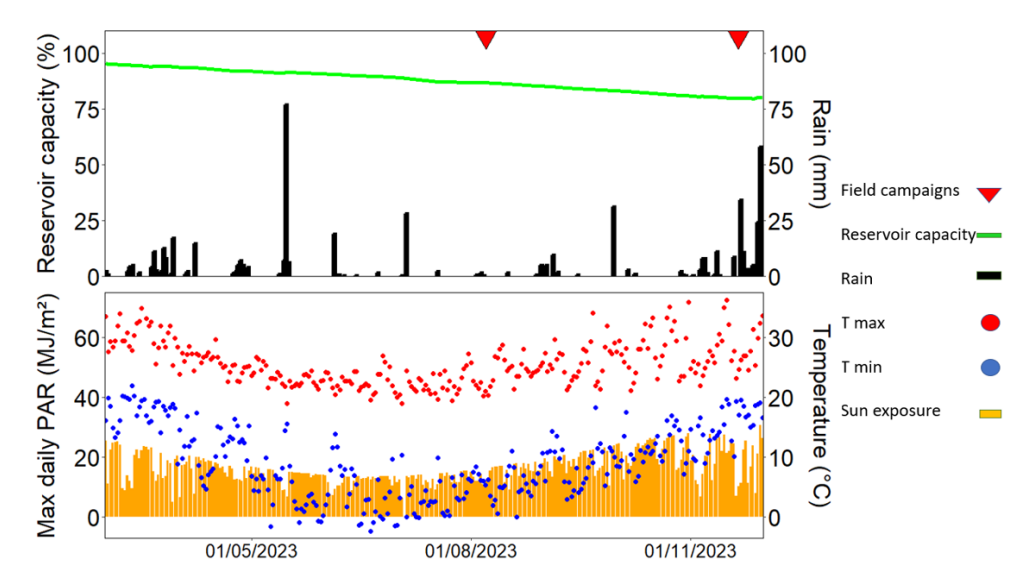
2.9 Statistical analyses

All reported errors represent standard errors of the mean. All analyses were undertaken using R (4.3.2). The Shapiro-Wilk normality test was used to determine if data was normally distributed (P<0.05). For normally distributed data, t-tests were applied to compared differences between groups. Otherwise, Wilcoxon rank-sum tests were used when data did not conform to normality. Differences between stem height measurements and between fluxes from the three plots were testes using Kruskal-Wallis One Way Analysis of Variance on Ranks, followed by the Dunn post hoc test for pairwise comparisons. Relationships between water depth and aquatic gas concentrations were assessed using linear models, where regression lines were fitted to log-transformed water depth.

3. Results

3.1 Site conditions

Reservoir water capacity declined during the two campaigns from 86% in winter to 80% in summer, resulting in a water level drop of ~1.5 m (Fig. 3). This was among the lowest levels since the dam wall was raised in 2011. Average water temperatures increased from 17.2 ± 0.1 °C in winter to 24.6 ± 0.7 °C during summer. Water temperature was similar between the top and bottom waters inside the ghost forest areas indicating no thermal stratification. The average maximum and minimum air temperature (including 14 days prior and after the fieldwork campaign) increased from 23.9 °C and 5.4 °C in winter, to 29.2 °C and 16.0 °C in summer. During the winter campaign, the reservoir received 1.5 mm of rain, while during the summer campaign 29 mm of precipitation occurred on the first two days and 4 mm over the rest of the week.



245 **Figure 3:** Climate and water level in Hinze Dam before and after sampling campaigns. Sun exposure (orange bars in MJ m⁻²) and rainfall (black bars in mm) were measured at the Hinze Dam weather station (ID 40847), while minimum (blue dots) and maximum (red dots) air temperature data (°C) were sourced from the Canungra weather



260



station (ID 140008). Reservoir capacity (%) data were obtained from Seqwater. The timing of the two sampling campaigns is marked by red triangles.

250 3.2 Water physicochemistry

Dissolved oxygen (DO%) in the water column of the reservoir was lower overall during winter than in summer (Table 1). The biggest change was observed at the southern site, where bottom DO increased from 60 to 90 % saturation between the two campaigns. The DO concentrations were 4, 3 and 11 % lower at the bottom of the water column compared to surface, in the North, Mid and South sites, respectively. During the summer campaign, the difference was 11, 21 and 27 % in the North, Mid and South sites, respectively. Surface water pH increased between campaigns, from 7.3 to 7.6, 7.3 to 7.9 and 7.2 to 8.3 for the North, Mid and South sites, respectively.

Table 1: Water physicochemical parameters at Hinze Dam for each of the three study sites (North, Mid, and South) for both surface and bottom water layers, in the different seasons. All averages are shown with \pm standard errors. * Only one measurement.

Site		Temperature °C		Ι	OO%	pН		
		Winter	Summer	Winter	Summer	Winter	Summer	
North	Surface	17.3 ± 0.13	23.9 ± 0.12	92.8 ± 0.12	106.8 ± 1.90	7.34 ± 1.27	7.68 ± 0.14	
	Bottom	17.4 *	23.9 ± 0.11	88.9 ± 0.17	95.42 ± 6.10	7.23 ± 1.73		
Mid	Surface	17.9 ± 0.10	24.4 ± 0.17	93.3 ± 0.05	109.3 ± 1.51	7.40 ± 0.48	7.95 ± 0.05	
	Bottom		24.5 ± 0.13	90.0 ± 0.07	105.5 ± 2.05	7.24 ± 0.69		
South	Surface	17.0 ± 0.06	25.4 ± 0.08	71.8 ± 0.06	117.9 ± 2.67	7.25 ± 0.10	8.37 ± 0.22	
	Bottom	16.8 ± 0.07	25.3 ± 0.05	60.2 ± 0.07	108.6 ± 5.12	6.90 ± 0.11		

3.3 Benthic sediment parameters

Benthic sediment organic carbon varied between sites, it was lowest at the South site (5.42 %) and highest at the Mid site (9.32 %) (Table 2). Phosphorus concentrations were the highest at the South site (963.3 mg/kg), more than double the other sites. The average uncorrected redox potential at the southern site ranged from -120 ± 12 to -113 ± 10 mV during the two campaigns, respectively. For the North site the average uncorrected redox potential shifted from -90 ± 12 to -53 ± 6 mV during summer. The Mid site had a larger variance in its uncorrected redox values during both campaigns, ranging from -121 to -85 mV on one shore to -17 to -1 mV on the opposite shore, inside the embayment. Similarly, during summer the redox potential ranged from -132 to -123 mV on one side to -62 and 53 mV on the other side of the bay. The sediments in the South site had the highest average oxygen demand (SOD) with 0.11 ± 0.001 mg O_2 ml⁻¹ d⁻¹. followed by the Mid site 0.08 ± 0.017 mg O_2 ml⁻¹ d⁻¹ and the North site 0.07 ± 0.009 mg O_2 ml⁻¹ d⁻¹.

265





Table 2: Benthic sediment characteristics at Hinze Dam at the North, Mid, and South study site locations. All averages are shown with ±SE.

Site	Uncorrected		SOD	Phosphorus	Carbon content	Organic
	Redox pot	ential (mV)				layer depth
			$(mg\ O_2 ml^{\text{-}1}\ d^{\text{-}1})$	(mg kg ⁻¹)	(% Corg)	(cm)
Campaign	Winter	Summer	Summer	Winter	Winter	Summer
North	-90.7 ± 11.8	-53 ± 6.1	0.07 ± 0.005	272 ± 27	6.82 ± 1.62	9
Mid	-61.3 ± 18.4	-59.2 ± 33.9	0.08 ± 0.01	452 ± 66	9.32 ± 0.89	8
South	-120.7 ± 12.3	-112.9 ± 9.5	0.11 ± 0.001	963 ± 68	5.42 ± 0.32	36

280 3.4 Tree density, size and water surface area

Measured tree DBH ranged from 17.0 to 37.5 cm, 19.7 to 60.0 cm and 18.0 to 41.8 cm for the North, Mid and Southern site, respectively. The average tree DBH per site was 30.2 ± 3.6 cm, 28.7 ± 3.5 and 23.5 ± 2.5 cm for the North, Mid and Southern site, respectively. The ghost forest tree density was 2200, 1350 and 1975 trees ha⁻¹ for the North, Mid and South sites, respectively. The tree basal areas covered between 1.5 and 2.5% of the water surfaces in the ghost forest areas. Tree height ranged from 10.0 to 28.8 m above the water surface and averaged 22.0 ± 2.7 m.

3.5 Aquatic CH₄ concentrations

285

290

Dissolved CH₄ concentrations in the surface water declined at our sample locations as the water depth increased during both winter ($r^2 = 0.28$, p < 0.005) and summer ($r^2 = 0.43$, p < 0.001) (Fig. 4). Aquatic CH₄ concentrations were highest during the summer campaign. There was no relationship between dissolved CO₂ and water depth for the winter ($r^2 = 0.01$, p = 0.59) nor the summer campaign ($r^2 = 0.03$, p = 0.38), although CO₂ concentrations were lower in summer compared to winter. This trend was less pronounced within the shallow ghost forest area.





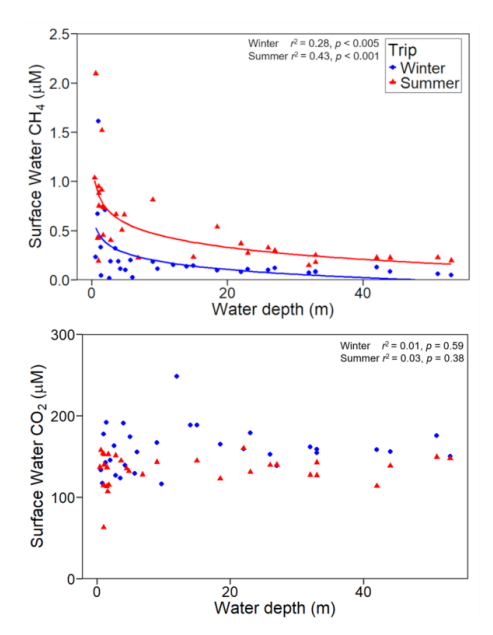


Figure 4: Surface water concentrations of dissolved CH_4 and CO_2 in Hinze Dam during the winter and summer campaigns. Data include samples from the three study sites (n = 6 per site) and a south-to-north transect (n = 12). Trend lines for significant relationships are shown.

3.6 Ebullition

295

300

305

There was considerable spatial and temporal heterogeneity in the ebullition CH₄ fluxes between, within and across sites. In winter, the average ebullition fluxes were 2253 ± 688 , 437 ± 104 and 2270 ± 819 µmol m⁻² d⁻¹ for the North, Mid and South sites, respectively (Fig. 5, Table 3). During the summer, average ebullition CH₄ fluxes were 1103 ± 339 , 1677 ± 427 and 6286 ± 1048 µmol m⁻² d⁻¹ for the North, Mid and South sites, respectively. There was a significant increase in ebullition flux between the winter and summer campaigns for the Mid (p < 0.05) and South site (p < 0.005). The decreased ebullition flux at the North site between winter and summer was not significant. For the winter campaign, the ebullition fluxes showed significant difference between the Mid and North site (p < 0.05), as well as the Mid and South site (p < 0.05). During the summer campaign we found significant differences in the ebullition fluxes between the South and North site (p < 0.005), as well as South and Mid site (p < 0.001).





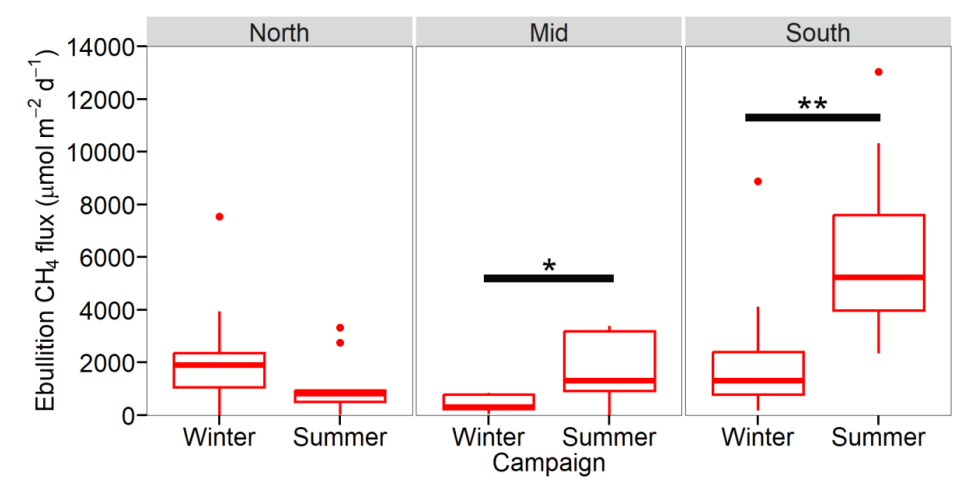


Figure 5: Average ebullition CH₄ fluxes (μmol m⁻² d⁻¹) with standard error from Hinze Dam, presented for the three sites (North, Mid, and South) during both winter and summer campaigns. Significant differences based on Wilcoxon tests are indicated with the solid black bar.

3.7 Aquatic CH₄ and CO₂ flux

310

315

320

325

Aquatic CH₄ diffusive flux rates differed between the three sites within the reservoir. During winter, the highest average aquatic CH₄ fluxes were measured at the North site $(264 \pm 25 \mu \text{mol m}^{-2} \text{ d}^{-1})$, followed by the South site $(131 \pm 41 \mu \text{mol m}^{-2} \text{ d}^{-1})$ and lowest at the Mid $(69.5 \pm 7.0 \mu \text{mol m}^{-2} \text{ d}^{-1})$ site (Fig. 6, Table 3). The North site showed significantly higher fluxes compared to the Mid site (p < 0.001) and to the South site (p < 0.005). During summer, the North had the highest average aquatic flux $(306 \pm 25 \mu \text{mol m}^{-2} \text{ d}^{-1})$ and Mid and South sites had similar fluxes $(218 \pm 51 \text{ and } 218 \pm 77 \mu \text{mol m}^{-2} \text{ d}^{-1})$. Significant differences were only observed between the North and South site (p < 0.01). Only the Mid site showed a significant increase in CH₄ aquatic fluxes between campaigns (p < 0.001).

Aquatic CO_2 fluxes were higher at the South site in both seasons. In winter, aquatic CO_2 fluxes were significantly higher at the South site ($50 \pm 8.5 \text{ mmol m}^{-2} \text{ d}^{-1}$) compared to the North ($18.5 \pm 1.8 \text{ mmol m}^{-2} \text{ d}^{-1}$, p < 0.001) and the Mid sites ($20.6 \pm 1.9 \text{ mmol m}^{-2} \text{ d}^{-1}$, p < 0.001). In summer, CO_2 aquatic fluxes were significantly lower during the summer campaign for all three sites (Fig. 6, South p < 0.001, Mid p < 0.001 and North p < 0.001). In addition, the South site still had the highest aquatic CO_2 flux ($11.7 \pm 3.3 \text{ mmol m}^{-2} \text{ d}^{-1}$), followed by the Mid ($5.1 \pm 1.2 \text{ mmol m}^{-2} \text{ d}^{-1}$) and North sites ($3.7 \pm 0.7 \text{ mmol m}^{-2} \text{ d}^{-1}$), with significant difference between the North and South site (p < 0.05).



355



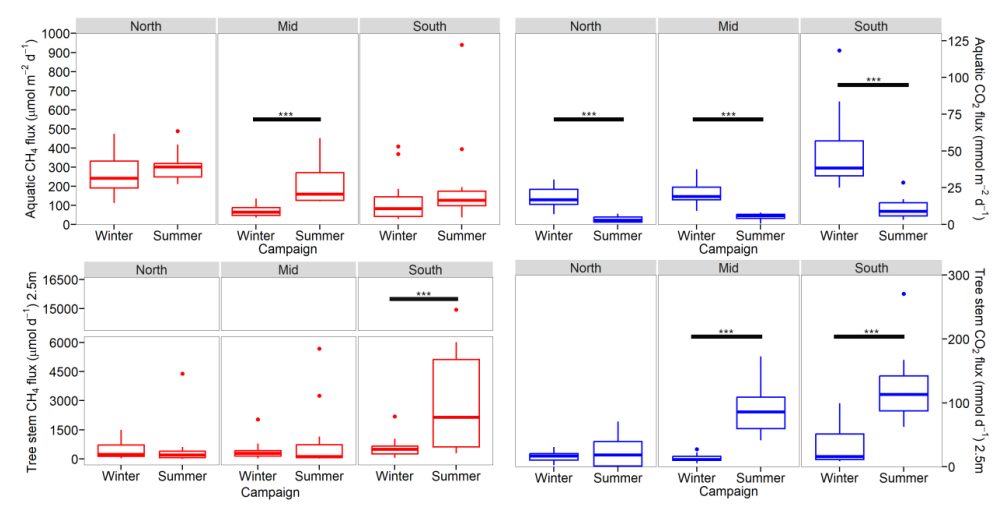


Figure 6: Aquatic diffusive CH_4 and CO_2 fluxes (left), and tree stem CH_4 fluxes (µmol tree⁻¹ d⁻¹) and carbon dioxide (CO_2) fluxes (mmol tree⁻¹ d⁻¹) (right). Tree fluxes were scaled to 2.5 m stem height, for all sampled trees in the three study sites of the Hinze Dam. Significant differences are shown with the solid horizontal line.

3.8 Ghost forest stem CH4 and CO2 fluxes

All trees and stem heights (total *n* = 192) emitted CH₄ and CO₂ during both campaigns. There was a high variability in the amount of CH₄ emitted per tree at all three sites. The CH₄ stem flux measurements ranged from 1.66 to 1584 μmol m⁻² d⁻¹ and 2.43 to 8614 μmol m⁻² d⁻¹ for the winter and summer campaigns, respectively (Fig. 6, Table 3). The CO₂ stem flux measurements ranged from 0.19 to 45.5 and 0.03 to 106 mmol m⁻² d⁻¹.

Average stem CH_4 fluxes per tree (upscaled to 2.5 m) were 510 ± 90 and 1770 ± 508 μ mol tree⁻¹ d^{-1} for the winter and summer campaign, respectively. The tree CH_4 fluxes ranged from 26.8 to 2196 μ mol tree⁻¹ d^{-1} during the winter campaign and from 5.34 to 14,944 μ mol tree⁻¹ d^{-1} in summer. The average CO_2 tree emissions (upscaled to 2.5 m) were 21.0 ± 3.4 and 81.6 ± 9.9 mmol tree⁻¹ d^{-1} for the winter and summer, respectively. The tree CO_2 fluxes ranged from 2.09 to 99.5 mmol tree⁻¹ d^{-1} during winter and 0.1 to 271 mmol tree⁻¹ d^{-1} during summer.

Average tree stem CH_4 fluxes were the highest in the South site during both campaigns (Fig. 4), winter 617 ± 162 and summer 3545 ± 1145 µmol tree⁻¹ d⁻¹ (Table 3), but only significantly different during the summer campaign (Mid-South p < 0.01 and North-South p < 0.005). The second highest tree fluxes were from the North site (453 ± 133 µmol tree⁻¹ d⁻¹) during the winter and the Mid site (1008 ± 524 µmol tree⁻¹ d⁻¹) during summer. Average tree stem CH_4 fluxes increased during the summer campaign, but were only significantly higher at the South site (p < 0.005).

Table 3: Summary of CH₄ fluxes from ghost forest tree stems, aquatic surfaces, and ebullition pathways during the winter (W) and summer (S) campaigns. For tree stems, the range of single measurements by stem height are included, along with the mean flux and total flux per hectare. For aquatic surfaces and ebullition, the mean flux and total flux per hectare are reported. All averages are shown with \pm standard errors.





Site	Camp aign	Stem height (cm)		Tree	ree stem flux		Aquatic flux		Ebullition flux	
			Min μmol m ⁻² d ⁻¹	Max μmol m ⁻² d ⁻¹	Mean μmol tree ⁻¹ d ⁻¹ (2.5m)	mol ha ⁻¹ d ⁻¹	Mean μmol m ⁻² d ⁻¹	mol ha ⁻¹ d ⁻¹	Mean μmol m ⁻² d ⁻¹	mol ha ⁻¹ d ⁻¹
North	W	0-60 60-120 120-200 ≥ 200	39.0 62.7 4.87 6.05	1068 1567 127 17.2	453 ± 133	1	264 ± 24.6	2.57	2252 ± 688	22
	S	0-60 60-120 120-200 ≤ 200	348 46.1 3.42 65.1	679 2339 1960 310	598 ± 367	1.32	306 ± 25.1	2.98	1102 ± 339	10.7
Mid	W	0-60 60-120 120-200 ≤ 200	1.66 1.83 12.3 44	1050 373 584 44	450 ± 163	0.61	69.5 ± 7	0.68	437 ± 104	4.3
	S	0-60 60-120 120-200 ≤ 200	5.96 12.2 2.43 29.7	1130 3039 3563 592	1008 ± 524	1.36	218 ± 51.4	2.14	1676 ± 427	16.5
South	W	0-60 60-120 120-200 ≤ 200	19.2 8.11 23 176	914 296 1507 471	617 ± 162	1.22	131 ± 40.6	1.29	2270 ± 819	22.3
	S	0-60 60-120 120-200 ≤ 200	30.4 43.1 31.8 47.8	2147 1335 8613 4873	3545 ± 1145	7	218 ± 77.4	2.15	6286 ± 1048	61.8

Average tree stem CO_2 fluxes were the highest in the South site for both campaigns, and increased significantly in summer (p < 0.005) from 31.9 ± 8.25 to 125 ± 15.3 mmol tree⁻¹ d⁻¹. CO_2 tree stem average fluxes in the North also increased significantly in summer (p < 0.001) from 16.3 ± 2.55 to 25.1 ± 7 µmol tree⁻¹ d⁻¹. In the Mid site average CO_2 fluxes increased from 13.9 ± 1.88 to 90.5 ± 11.1 µmol tree⁻¹ d⁻¹. During summer the CO_2 tree stem fluxes were significant higher in the Mid and South site, compare to the North site (Mid-North p < 0.005 and South-North p < 0.001).

3.9 Flux versus stem height

360

365

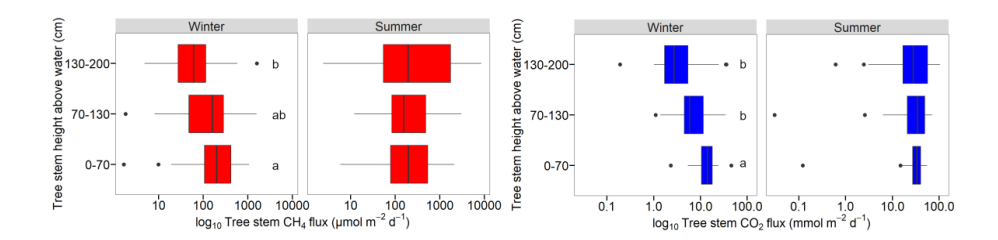
370

In winter, the ghost forest stem CH₄ fluxes decreased with stem height. The average flux rates were 318 ± 55.8 , 251 ± 57.0 and 153 ± 54 µmol m⁻² d⁻¹ for the lower, middle and upper measurements (Fig. 7), with the lower and upper stem height fluxes being significantly different (p < 0.005). One tree at the South site showed the highest flux of the campaign (1507 µmol m⁻² d⁻¹), however, the flux chamber was located over a stem fissure. The same trend was observed for CO₂, as average stem height fluxes decreased from 15.1 ± 1.5 , 8.5 ± 1.4 and 7.64 ± 2.3 mmol m⁻² d⁻¹ for the lower, middle and upper stem measurements, with significant differences between the lower measurement, versus the middle (p < 0.005) and upper stems (p < 0.001).



390



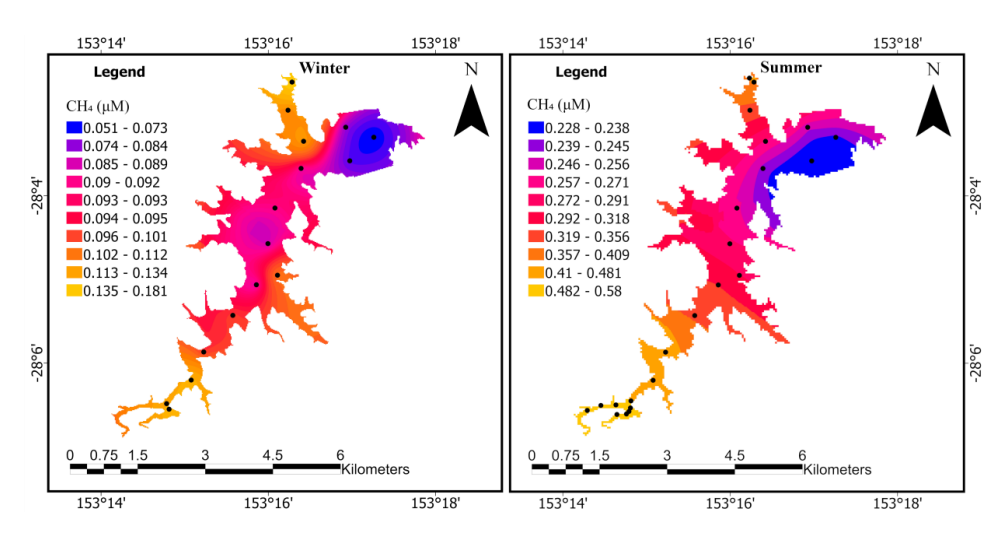


375 **Figure 7:** Tree stem CH₄ (in μmol m⁻² d⁻¹) and CO₂ (in mmol m⁻² d⁻¹) fluxes measured at three heights (cm) above water level at Hinze Dam. Data are presented for the three study sites during both winter and summer campaigns. The figure includes groupings based on results from Dunn's test for statistical comparisons.Note: log scale for x-axis.

In summer, no significant differences between stem heights were found (Fig. 7), however the highest average CH₄ flux observed was at the uppermost measurement ($1224 \pm 409 \, \mu \text{mol m}^{-2} \, d^{-1}$), especially at the South site. Similarly, CO₂ fluxes did not show significant changes with stem height during the summer campaign. The internal tree stem gas samples (n=14) contained an average CH₄ concentration of $51,086 \pm 10,126 \, \text{ppm}$ (or $5.1 \, \%$ saturation), being four orders of magnitude higher than the atmosphere.

3.10 Upscaling CH₄ emission pathways within the total reservoir

The surface water CH_4 concentrations decreased from south to north, during both campaigns (Fig. 8). Up scaling CH_4 fluxes to the whole reservoir showed that total CH_4 emissions tripled between the winter and summer campaigns, from 1418 to 4604 mol d^{-1} (Table 4). Tree stem CH_4 emissions tripled between the two campaigns, from 207 to 628 mol d^{-1} and contributed 14 % and 15 % in winter and summer respectively. Overall, ebullition was the dominant CH_4 emission source (67 % in winter and 58 % in summer), while aquatic fluxes from the deeper open water contributed only 2 % and 13 % for winter and summer, with aquatic fluxes of the shallow ghost forested areas contributed 16 % and 14 % respectively.







395 **Figure 8:** Surface water CH₄ (μM) concentrations in the western part of Hinze Dam, Australia. Samples were taking along a transect from south to north in 1 km intervals (black dots), during the winter (left) and summer (right) campaign.

Table 4: Upscaled CH₄ flux estimates for the total area of Hinze Dam, incorporating all three emission pathways.

Campaign	Total CH ₄ flux (mol d ⁻¹)	Ghost forest tree stem flux (2.5m)	Ghost forest aquatic flux	Ebullition flux (to 8m)	Open water aquatic flux			
	iiux (IIIOI u)	% (CH ₄ mol d ⁻¹)						
Winter	1418	15 (207 ± 70)	16 (232 ± 24)	67 (949 ± 163)	2 (31)			
Summer	4604	$14~(628\pm241)$	$14~(647\pm135)$	$58~(2694\pm485)$	14 (636)			

400 4. Discussion

405

410

415

420

425

4.1 Seasonal variability of aquatic and ebullition fluxes

Overall, there were three-fold higher CH₄ fluxes observed during the summer campaign, along with elevated dissolved CH₄ concentrations and ~7° C increase in surface water temperature, particularly in the south site. This temperature change likely increased microbial metabolism, including methanogenesis and, therefore resulting in higher rates of CH₄ production. This was further evidenced as ebullition rates also increased in both the Mid and South sites, during summer. Temperature has been shown to enhance CH₄ flux rates (Yvon-Durocher et al., 2014) and increased ebullition in summer across multiple lake systems (Sanches et al., 2019; Aben et al., 2017). Sediments from boreal and temperate lakes have shown an exponential increase in CH₄ production and released more CH₄ with temperature increase every 6°C (Liikanen, 2002; Duc et al., 2010). Previous studies have found higher ebullition fluxes above 30°C compared to below 20°C (Xun et al., 2024). In contrast, other studies have found that ebullition has no significant positive correlation with water temperature (Grinham et al., 2018b), suggesting organic matter content and water level changes as more important drivers. Ebullition release can also be influenced by sudden atmospheric pressure changes and wind driven turbulence (Kellner et al., 2006; Tokida et al., 2007). Aside from seasonal variability, ebullition bubble release events are highly heterogeneous (Walter Anthony K. M. and Anthony, 2013) and temporally variable (Linkhorst et al., 2020) making them a difficult CH₄ flux term to accurately constrain (Rosentreter et al., 2021).

The CO₂ aquatic fluxes and dissolved CO₂ concentrations declined from winter to summer. CO₂ fluxes typically display high diel variability, especially in tropical regions, where most CO₂ emissions occur at night due respiration, contrasting lower CO₂ from photosynthesis occurring during the day (Reis and Barbosa, 2014). In summer, the daylight hours are longer and higher temperatures can increase primary production from phytoplankton and algae in the water (Yang et al., 2015). Primary production consumes CO₂ and produces O₂, which corresponds with the increase in dissolved oxygen we observed in the water column during our summer campaign. The aquatic surface CH₄ concentration was lower in the deep reservoir central basin, compared to the shallower ghost forested embayments. Deeper water results in a longer residence time of CH₄ within the water column, allowing for greater oxidation of CH₄. Up to 80% of CH₄ being produced in deep water sediments can

https://doi.org/10.5194/egusphere-2025-5594 Preprint. Discussion started: 19 November 2025 © Author(s) 2025. CC BY 4.0 License.



445

450

455

460



be oxidized, while CH₄ produced in shallower zones undergoes less oxidation prior to being emitted to the atmosphere (Bastviken et al., 2008).

4.2 Spatial variability of CH₄ fluxes

430 CH₄ dynamics showed notable differences among the three investigated sites, suggesting site specific factors driving CH₄ fluxes. Although temperature is a key factor, it is not the only factor influencing CH₄ concentration and fluxes. Site orientation and adjacent bathymetry affect both the amount of sun and wind, in turn influencing site physicochemical conditions. The South site showed the highest ebullition and tree stem fluxes between all three sites. The South site is located at the inflow into the reservoir through the Nerang River, resulting in fresh 435 organic matter being deposited into this section of the reservoir. Even though the organic carbon concentration in the sediment was similar between the three sites, the depth of the organic layer in the South site was ~3-fold deeper (<30 cm compared to >10 cm), leading to greater substrate availability for methanogenesis, likely explaining the higher tree and ebullition CH₄ fluxes observed. Similar to our findings, a study at nearby Little Nerang Dam, Australia (upstream from the eastern inflow), found that the ebullition fluxes were driven by 440 sediment organic matter content, especially at the inflow site (Grinham et al., 2018b). Other studies have reported organic matter availability influencing ebullition CH₄ fluxes (Casper, 2000; Sobek et al., 2012) and have shown higher ebullition at inflow sites in a reservoir in Zambia (Delsontro et al., 2011), Czech Republic (Tušer et al., 2017) and in China (Shi et al., 2025). A previous study at Hinze Dam, before the dam was raised, also found the highest fluxes in the south-west of the reservoir at the same inflow site (Sherman and Ford, 2011).

The lability of the carbon in the organic material and the microbial community in the sediments should also be considered. Studies have found that CH₄ production is closely linked to the degradability of the organic material (Praetzel et al., 2020; Grasset et al., 2018; Zhou et al., 2025). Phosphorus is also an important nutrient for microbial growth. The South site sediment had the highest phosphorus concentration, which has been linked to increased primary and higher CH₄ production (Bastviken et al., 2004). In addition, another proxy for microbial activity and organic matter lability is the sediment oxygen demand (SOD). During the summer SOD was highest at the South site, further confirming the assumption that there is more easily degradable organic material and higher microbial activity within the sediment. Our findings also show lower aquatic dissolved oxygen concentration at the bottom of the water column and the lowest dissolved oxygen concentration at the South site. Oxygen consumption and the resulting depletion in the water column is usually driven more by SOD in shallow aquatic ecosystems, than

water column oxygen consumption (Macpherson et al., 2007; Caldwell and Doyle, 1994).

4.3 Drivers of ghost forest tree stem CH₄ and CO₂ fluxes

All trees emitted CH_4 and CO_2 during both campaigns and from all three measured stem heights. We observed high variation between the fluxes of the different trees undergoing different stages of decomposition, and due to the influence of the stem fissures and bark remnants (Jeffrey et al., 2020b). Cracks result from the decomposition and drying of the dead trees (Oltean L. et al., 2007). All sampled trees died at around the same time in 2011 as the water levels rose due to the raising of the dam wall. Due to their state of decomposition, we could not identify the tree species, but different species can have different decomposition speeds (Freschet et al., 2012; Kahl et al., 2017). Many of large trees were likely *Eucalyptus* sp. based on the species in the adjacent areas located above the





475

480

485

dam maximum water level. *Eucalyptus* sp. are classified as hardwoods (Fao, 2002) and therefore are somewhat more resistant to decomposition. Previous studies have found high variance in tree CH₄ fluxes even of the same species, in living (Jeffrey et al., 2023) and dead trees (Warner et al., 2017; Kipping et al., 2022). Decomposition stages effects both CH₄ (Covey et al., 2016) and CO₂ fluxes (Kipping et al., 2022). This leads to high variations between all measured tree stem fluxes and explains the high variability for both CH₄ and CO₂.

During the winter campaign, CH₄ and CO₂ fluxes declined with stem height, consistent with gas diffusion observations from living wetland trees, which are ecosystems featuring strong soil CH₄ and CO₂ sources (Jeffrey et al., 2023; Jeffrey et al., 2020a; Pangala et al., 2017; Sjogersten et al., 2020). Previous studies focused on dead tree axial trends, found that CH₄ and CO₂ also decreased in stem concentration, and with increasing stem height (Carmichael and Smith, 2016; Carmichael et al., 2018; Jeffrey et al., 2020b). However, they did not find a significant difference in flux rate due to low sample size (two heights and n=8). δ^{13} C-CH₄ measurements in dead trees suggest that CH₄ may be oxidized while moving upwards within tree stems, suggesting a soil source (Martinez et al., 2022). This soil source of CH4 is further supported by research that has found that wood samples produced little CH₄ during anaerobic incubations (Martinez et al., 2022). In our study, the dead trees were in several metres of standing freshwater, featuring low-oxgyen and high BOD soil conditions. It is therefore possible that the majority of CH₄ and CO₂ originates from the sediments (with the trees acting as passive gas conduits), that diffuses outwards with increasing stem height. Nevertheless, due to different decomposition rates, we cannot rule out that internal microbial production of CH₄ may contribute to some of the CH₄ and CO₂ flux observed. The opposite trend was observed for both CH₄ and CO₂ during summer, with the highest fluxes occurring at the highest stem height. The water level had dropped ~1.5 m between the two campaigns, thus potentially changing the preferential pathway of CH₄ and CO₂ emissions higher up the tree stems. We acknowledge that further factors, like wood water content or changing internal CH₄ and CO₂ production and oxidation likely also played a role. Nevertheless, our summer results do not necessarily point to a wood source, but rather show the complexity of tree stem fluxes in such a dynamic system.

In living trees, it has recently been shown that CH₄ (gas phase) can travel rapidly through the bark of some wetland species, separate to the transport within the transpiration stream (liquid phase) (Jeffrey et al., 2024). Because dead trees no longer have bark and lack an active transpiration stream, this suggests that diffusion through cracks and open spaces through the dead wood may have been a more important pathway for CH₄ egress (gas phase) to be released from the reservoir sediments. However, the wood below the water line was saturated and thus reduced CH₄ diffusion rates (dissolved phase), being several orders of magnitude slower than gas. This may have lead to a lag time between CH₄ production changes within the soil, and stem CH₄ gas emissions above the waterline. Further research is required to confirm both the CH₄ source(s), the transport rates and preferential pathway(s) for ghost forests.

We found no correlation between surface water depth and tree stem CH₄ flux (Fig. S3). This was similar to riparian living tree studies in the Amazon (Gauci et al., 2022) and Australia (Jeffrey et al., 2023) which found that as the below-ground water table rose, it promoted anaerobic conditions in the soil, leading to increased CH₄ production and, consequently, higher tree fluxes. However, once surface inundation occurred, further increases in surface water depth did not significantly alter soil conditions, and therefore tree CH₄ fluxes remained similar. For the



515

520

525



flooded ghost forest, as stem CH₄ fluxes were decoupled from variation in surface water depth, this likely reflected the dominance of soil CH₄ production, stem wood properties and decomposition state, over hydrological controls.

4.4 Comparison with other studies

Compared to previous ghost forest CH_4 studies, our average CH_4 stem fluxes were within the reported range (Table 5). However, it should be noted that each study considered a different amount of stem height measurements (Jeffrey et al. 2019 = 4, Carmichael et al. 2018 & 2024 = 1 & 2, Martinez et al. 2022 = 1 and our study = 3). As CH_4 fluxes can change with stem height, the height and number of heights measured can strongly influence estimated fluxes. On tree in our study emitted the highest single flux from a dead tree, almost twice that of previous maxima (Table 5), highlighting potential for extreme heterogeneity. One reason our higher CH_4 fluxes may occur is because our study was located within a subtropical region, featuring higher CH_4 production and fluxes, compared to temperate climates. Although Jeffrey et al. (2019) studied mangroves in tropical regions, seawater-derived sulphate in mangrove ecosystems likely lowered soil CH_4 production. Sulphate and iron reducers can outcompete methanogens for H_2 or acetate when sulphate and iron are available (Roden and Wetzel, 2002). Similarly, salinity and sulphate on coastal forests can influence soil CH_4 production (Martinez and Ardón, 2021) and reduce tree CH_4 fluxes. Our study showed that the site conditions in a freshwater reservoir ghost forest were favourable for high CH_4 production.

Table 5: Comparison of average and maximum CH_4 and CO_2 fluxes from dead tree stems and stem debris between this study and previous studies. For Jeffrey et al. 2019, only fluxes from dead mangroves are included, while for Martinez et al. 2021 and both Carmichael et al. 2018 and 2024 studies, only positive fluxes are presented. The highest reported mean stem CH_4 concentration per study is presented here.

Publication	Height measurements	C	CH4	CO_2		Stem concentration	
	n (cm)	Mean	Highest	Mean	Highest	Highest Mean	
		$\mu mol\ m^{\text{-}2}\ d^{\text{-}1}$	μ mol m ⁻² d ⁻¹	mmol m ⁻² d ⁻	mmol m ⁻² d ⁻	CH ₄ ppm	
Carmichael and Smith 2016						104 ±19	
Covey et al. 2016						286.4 ±148	
Carmichael et al. 2018	2 (10, 60)	599 ± 150	1044	62 ± 13	123	78	
Jeffrey et al. 2019	4 (10, 40, 80, 170)	249 ± 41.0	4035			64,056	
Martinez et al.2021	1 (60)	449 ± 135	4644	63 ± 8.17	603		
Martinez et al. 2022						904 ±415	
Carmichael et al. 2024	1 (30, 60, 120)	314 ± 224	763			23.7 ± 7.5	
Our study	3 (20, 100, 180)	465 ± 76	8613	23.7 ± 1.63	106	51,086 ± 10,127	

https://doi.org/10.5194/egusphere-2025-5594 Preprint. Discussion started: 19 November 2025 © Author(s) 2025. CC BY 4.0 License.



530

535

540

545

560



Internal stem CH₄ gas concentrations were similar to that of subtropical dead mangroves, but higher than the other studies. This may be attributed to the longer incubation period (24 h) used in our study, compared to others, which typically have incubation times under one hour. Additionally, our stem gas concentrations were collected during the summer campaign, when higher tree fluxes and potentially elevated stem gas concentrations were observed likely due to increased microbial activity. Importantly, we did not observe any uptake of CH₄ which had previously been observed in ghost forests (Martinez and Ardón, 2021). Previous studies measured net CH₄ uptake in 38% and 20% of their measurements, respectively (Carmichael et al., 2024; Carmichael et al., 2018). Carmichael et al. (2024) found sequencing based evidence for methanotroph communities inside dead trees, showing the potential oxidation capacity, whilst our results suggest that net CH₄ emissions exceeded any CH₄ oxidation.

4.5 Importance of ghost forest tree stem CH₄ emissions

Our study reveals that reservoir ghost forests can emit a significant amount of CH₄ to the atmosphere. Studies have found herbaceous (non-woody) plant-mediated diffusion can dominate shallow aquatic CH₄ fluxes, with ebullition only playing a minor role (Jeffrey et al., 2019a; Whiting and Chanton, 1992; Chanton et al., 1992; Bastviken et al., 2022). However, in small and shallower lakes in Europe, and ponds in Australia, ebullition was determined to be the primary CH₄ source to the atmosphere (Schmiedeskamp et al., 2021; Grinham et al., 2018a). Indeed, ebullitive fluxes have been estimated to account for 80% of the total reservoir flux globally (Johnson et al., 2021), especially within (sub)tropical regions (Harrison et al., 2021). Our subtropical ebullition rates were the largest contributor to overall CH₄ fluxes at 58% and 67%. Despite our deployment strategy (and daily sampling) of ~60 ebullition chambers, spanning three sites and various water depth gradients - our sampling approach is still seasonally limited, therefore remains challenging to draw a definitive conclusion. Greater temporal and spatial sampling approaches would reduce these uncertainties and better constrain this CH₄ flux term.

However, tree stem CH₄ contributions of 15% and 14% during winter and summer, respectively, suggest a consistent, and substantial CH₄ source. We acknowledge that extrapolating reservoir-wide emissions from only three sites should be considered with caution, particularly given the absence of data from the eastern part of the reservoir. However, tree stem upscaling was done conservatively to only 2.5 m of stem height, therefore ghost forest CH₄ flux contribution may well be underestimated. Future studies should therefore explicitly account for ghost forest tree emissions to improve the accuracy of reservoir greenhouse gas budgets. Furthermore, because we used the Mid site—which exhibited lower emissions compared to the other sites—to scale up for large areas of the reservoir, our approach likely results in a conservative estimate of ebullition and total emission.

5.1 Conclusions

This study advances our understanding of seasonal changes influencing reservoir CH₄ fluxes, and provide the first estimates of ghost forest tree stem emissions and their contribution to the total reservoir CH₄ budget. Our findings reveal high system variability and potential CH₄ local hotspots inside reservoirs at inflow zones, where higher organic matter availability and temperature-driven microbial activity likely enhance CH₄ production. These results





emphasize the contribution of ghost forests fluxes in reservoir greenhouse gas budgets and can help guide future management decisions around ghost forest creation.

565

570

575

We demonstrated that ghost forests can play a crucial role in reservoir greenhouse gas emissions and where present, they should be accounted for in reservoir greenhouse gas budgets. We suggest that the major source of tree stem CH₄ emissions likely come from the soil, but further research incorporating microbial genetic sequencing, stable isotope tracing and wood and soil incubations would be necessary to confirm this. Additional research is required to further understand changing CH₄ and CO₂ hotspots on stems during the seasons.

Aside from greenhouse gas emissions, ghost forests also provide other important ecosystem functions. They serve as habitat for birds and fish for hunting and nesting. However, quantifying these benefits against potential greenhouse gas emissions is challenging. Future management decisions should carefully assess the costs and benefits associated with removing the trees during reservoir construction stages. Despite the increasing body of research on tree CH₄ fluxes, substantial knowledge gaps remain, particularly concerning ghost forests and tree mortality. These unique ecosystems are expected to become more prevalent due to climate change and other anthropogenic modifications of ecosystems, underscoring the critical importance of further investigations and haseline information

580

595

600

Data availability: The flux data is available as online repositories from the 30.03.2026 at doi:10.17632/vryhr6gcxr.1 (Dittmann, 2025) and can also be requested from Johannes Dittmann (j.dittmann.10@student.scu.edu.au).

Author contribution: L.C.J, J.D., D.M. and S.J. conceived and designed the study. J.D., L.C.J., S.J., D.T., A.G., P.G.A. and D.M. conducted all fieldwork. J.D. wrote the first draft. All authors contributed to the final manuscript.

Competing interests: The authors declare that they have no conflict of interest.

Acknowledgements: I thank Sequater for assistance with access to the field site and providing information on the bathymetry and history of Hinze Dam.

Financial support: This research was supported by research grants from the Australian Research Council (DE240100338 to L.C.J; DP210100096 to D.T.M); an Australian Institute of Nuclear Science and Engineering (AINSE) PGRA (to J.D.); Holsworth Wildlife Research Endowment fund (to J.D.); The Hermon Slade Foundation (to L.C.J., D.T.M., S.G.J.) and an AINSE ECRA (to L.C.J.).

6. References

Aben, R. C. H., Barros, N., van Donk, E., Frenken, T., Hilt, S., Kazanjian, G., Lamers, L. P. M., Peeters, E. T. H. M., Roelofs, J. G. M., de Senerpont Domis, L. N., Stephan, S., Velthuis, M., Van de Waal, D. B., Wik, M., Thornton, B. F., Wilkinson, J., DelSontro, T., and Kosten, S.: Cross continental increase in methane ebullition under climate change, Nat. Commun., 8, 1682, https://doi.org/10.1038/s41467-017-01535-y, 2017.



620

625

630



- Barba, J., Bradford, M. A., Brewer, P. E., Bruhn, D., Covey, K., van Haren, J., and al., e.: Methane emissions from tree stems: a new frontier in the global carbon cycle, New Phytol., 222, 18-28, https://doi.org/10.1111/nph.15582, 2019.
- Barba, J., Brewer, P. E., Pangala, S. R., and Machacova, K.: Methane emissions from tree stems current knowledge and challenges: an introduction to a Virtual Issue, New Phytol., 241, 1377-1380, https://doi.org/10.1111/nph.19512, 2024.
- Bastviken, D., Cole, J., Pace, M., and Tranvik, L.: Methane emissions from lakes: Dependence of lake characteristics, two regional assessments, and a global estimate, Glob. Biogeochem. Cycles, 18, GB4009, https://doi.org/10.1029/2004gb002238, 2004.
 - Bastviken, D., Cole, J. J., Pace, M. L., and Van de Bogert, M. C.: Fates of methane from different lake habitats: Connecting whole-lake budgets and CH4 emissions, J. Geophys. Res. G: Biogeosci., 113, G02024, https://doi.org/10.1029/2007jg000608, 2008.
- Bastviken, D., Treat, C. C., Pangala, S. R., Gauci, V., Enrich-Prast, A., Karlson, M., and al., e.: The importance of plants for methane emission at the ecosystem scale, Aquat. Bot., 184, 103596, https://doi.org/10.1016/j.aquabot.2022.103596, 2022.
 - Boucher, O., Friedlingstein, P., Collins, B., and Shine, K. P.: The indirect global warming potential and global temperature change potential due to methane oxidation, Environ. Res. Lett., 4, 0440077, https://doi.org/10.1088/1748-9326/4/4/044007, 2009.
 - Caldwell, J. M. and Doyle, M. C.: Sediment Oxygen Demand in the Lower Willamette River, Oregon, United States Geological Survey Water-Resources Investigations Report 95–4196, 1-14, https://doi.org/, 1994.
 - Carmichael, M. J., Bernhardt, E. S., Bräuer, S. L., and Smith, W. K.: The role of vegetation in methane flux to the atmosphere: should vegetation be included as a distinct category in the global methane budget?, Biogeochemistry, 119, 1-24, https://doi.org/10.1007/s10533-014-9974-1, 2014.
 - Carmichael, M. J. and Smith, W. K.: Standing Dead Trees: a Conduit for the Atmospheric Flux of Greenhouse Gases from Wetlands?, Wetlands, 36, 1183-1188, https://doi.org/10.1007/s13157-016-0845-5, 2016.
 - Carmichael, M. J., Helton, A. M., White, J. C., and Smith, W. K.: Standing Dead Trees are a Conduit for the Atmospheric Flux of CH4 and CO2 from Wetlands, Wetlands, 38, 133-143, https://doi.org/10.1007/s13157-017-0963-8, 2018.
 - Carmichael, M. J., Martinez, M., Brauer, S. L., and Ardon, M.: Microbial Communities in Standing Dead Trees in Ghost Forests are Largely Aerobic, Saprophytic, and Methanotrophic, Curr. Microbiol., 81, 229, https://doi.org/10.1007/s00284-024-03767-w, 2024.
 - Chanton, J., P., Whiting, G., J., Showers, W. J., and Crill, M. P.: Methane Flux from Peltandra Virginica: Stable Isotope Tracing and Chamber Effects, Glob. Biogeochem. Cycles, 6, 15-31, https://doi.org/, 1992.
 - Covey, K. R., Bueno de Mesquita, C. P., Oberle, B., Maynard, D. S., Bettigole, C., Crowther, T. W., Duguid, M. C., Steven, B., Zanne, A. E., Lapin, M., Ashton, M. S., Oliver, C. D., Lee, X., and Bradford, M. A.: Greenhouse trace gases in deadwood, Biogeochemistry, 130, 215-226, https://doi.org/10.1007/s10533-016-0253-1, 2016.
- 640 Covey, K. R. and Megonigal, J. P.: Methane production and emissions in trees and forests, New Phytol., 222, 35-51, https://doi.org/10.1111/nph.15624, 2018.
 - DelSontro, T., Kunz, M. J., Kempter, T., Wuest, A., Wehrli, B., and Senn, D. B.: Spatial heterogeneity of methane ebullition in a large tropical reservoir, Environ. Sci. Technol., 45, 9866-9873, https://doi.org/10.1021/es2005545, 2011.
- Dittmann, J.: Dataset supporting the manuscript: "Are ghost forests a substantial source of methane from reservoirs?", Mendeley Data [dataset], https://doi.org/10.17632/vryhr6gcxr.1 2025.
 - Duc, N. T., Crill, P., and Bastviken, D.: Implications of temperature and sediment characteristics on methane formation and oxidation in lake sediments, Biogeochemistry, 100, 185-196, https://doi.org/10.1007/s10533-010-9415-8, 2010.
- 650 FAO: Case Study on Long Rotation Eucalypt Plantations in New South Wales by R. Heathcote, Forest Plantations Working Paper 22, 2002.
 - Freschet, G. T., Weedon, J. T., Aerts, R., van Hal, J. R., and Cornelissen, J. H. C.: Interspecific differences in wood decay rates: insights from a new short-term method to study long-term wood decomposition, J. Ecol., 100, 161-170, https://doi.org/10.1111/j.1365-2745.2011.01896.x, 2012.
- Friedlingstein, P., O'Sullivan, M., Jones, M. W., Andrew, R. M., Hauck, J., Olsen, A., and Peters, G. P., Peters, W., Pongratz, J., Sitch, S., Le Quéré, C., Canadell, J. G., Ciais, P., Jackson, R. B., Alin, S., Aragão, L. E. O. C., Arneth, A., Arora, V., Bates, N. R., Becker, M., Benoit-Cattin, A., Bittig, H. C., Bopp, L., Bultan, S., Chandra, N., Chevallier, F., Chini, L. P., Evans, W., Florentie, L., Forster, P. M., Gasser, T., Gehlen, M., Gilfillan, D., Gkritzalis, T., Gregor, L., Gruber, N., Harris, I., Hartung, K., Haverd, V.,
- Houghton, R. A., Ilyina, T., Jain, A. K., Joetzjer, E., Kadono, K., Kato, E., Kitidis, V., Korsbakken, J. I., Landschützer, P., Lefèvre, N., Lenton, A., Lienert, S., Liu, Z., Lombardozzi, D., Marland, G., Metzl, N., Munro, D. R., Nabel, J. E. M. S., Nakaoka, S.-I., Niwa, Y., O'Brien, K., Ono, T., Palmer, P. I., Pierrot,



685

695



- D., Poulter, B., Resplandy, L., Robertson, E., Rödenbeck, C., Schwinger, J., Séférian, R., Skjelvan, I., Smith, A. J. P., Sutton, A. J., Tanhua, T., Tans, P. P., Tian, H., Tilbrook, B., van der Werf, G., Vuichard, N., Walker, A. P., Wanninkhof, R., Watson, A. J., Willis, D., Wiltshire, A. J., Yuan, W., Yue, X., and Zaehle, S.: Global Carbon Budget 2020, Earth Syst. Sci. Data, 12, 3269-3340, https://doi.org/10.5194/essd-12-3269-2020, 2020.
 - Gauci, V., Figueiredo, V., Gedney, N., Pangala, S. R., Stauffer, T., Weedon, G. P., and Enrich-Prast, A.: Non-flooded riparian Amazon trees are a regionally significant methane source, Philosophical Transactions of the Royal Society A, 380, 20200446, https://doi.org/10.1098/rsta.2020.0446, 2022.
 - Grasset, C., Mendonca, R., Saucedo, G. V., Bastviken, D., Roland, F., and Sobek, S.: Large but variable methane production in anoxic freshwater sediment upon addition of allochthonous and autochthonous organic matter, Limnol. Oceanogr., 63, 1488-1501, https://doi.org/10.1002/lno.10786, 2018.
- Grinham, A., Albert, S., Deering, N., Dunbabin, M., Bastviken, D., Sherman, B., Lovelock, C. E., and Evans, C.

 D.: The importance of small artificial water bodies as sources of methane emissions in Queensland,
 Australia, Hydrol. Earth Syst. Sci., 22, 5281-5298, https://doi.org/10.5194/hess-22-5281-2018, 2018a.
 - Grinham, A., Dunbabin, M., and Albert, S.: Importance of sediment organic matter to methane ebullition in a subtropical freshwater reservoir, Sci. Total Environ., 621, 1199-1207, https://doi.org/10.1016/j.scitotenv.2017.10.108, 2018b.
- Harrison, J. A., Prairie, Y. T., Mercier-Blais, S., and Soued, C.: Year-2020 Global Distribution and Pathways of Reservoir Methane and Carbon Dioxide Emissions According to the Greenhouse Gas From Reservoirs (G-res) Model, Glob. Biogeochem. Cycles, 35, https://doi.org/10.1029/2020gb006888, 2021.
 - Hu, Z., Xu, C., McDowell, N. G., Johnson, D. J., Wang, M., Luo, Y., Zhou, X., and Huang, Z.: Linking microbial community composition to C loss rates during wood decomposition, Soil Biol. Biochem., 104, 108-116, https://doi.org/10.1016/j.soilbio.2016.10.017, 2017.
 - Jeffrey, L. C., Maher, D. T., Johnston, S. G., Kelaher, B. P., Steven, A., and Tait, D. R.: Wetland methane emissions dominated by plant-mediated fluxes: Contrasting emissions pathways and seasons within a shallow freshwater subtropical wetland, Limnol. Oceanogr., 64, 1895-1912, https://doi.org/10.1002/lno.11158, 2019a.
- 690 Jeffrey, L. C., Reithmaier, G. M., Sippo, J. Z., Johnston, S. G., Tait, D. R., Harada, Y., and Maher, D. T.: Are methane emissions from mangrove stems a cryptic carbon loss pathway? Insights from a catastrophic forest mortality, New Phytol., 224, 146-154, https://doi.org/10.1111/nph.15995, 2019b.
 - Jeffrey, L. C., Maher, D. T., Tait, D. R., Euler, S., and Johnston, S. G.: Tree stem methane emissions from subtropical lowland forest (Melaleuca quinquenervia) regulated by local and seasonal hydrology, Biogeochemistry, 151, 273-290, https://doi.org/10.1007/s10533-020-00726-y, 2020a.
 - Jeffrey, L. C., Maher, D. T., Tait, D. R., and Johnston, S. G.: A Small Nimble In Situ Fine-Scale Flux Method for Measuring Tree Stem Greenhouse Gas Emissions and Processes (S.N.I.F.F), Ecosystems, 23, 1676-1689, https://doi.org/10.1007/s10021-020-00496-6, 2020b.
- Jeffrey, L. C., Moras, C. A., Tait, D. R., Johnston, S. G., Call, M., Sippo, J. Z., Jeffrey, N. C., Laicher-Edwards, D., and Maher, D. T.: Large Methane Emissions From Tree Stems Complicate the Wetland Methane Budget, J. Geophys. Res. G: Biogeosci., 128, https://doi.org/10.1029/2023jg007679, 2023.
 - Jeffrey, L. C., Johnston, S. G., Tait, D. R., Dittmann, J., and Maher, D. T.: Rapid bark-mediated tree stem methane transport occurs independently of the transpiration stream in Melaleuca quinquenervia, New Phytol., 242, 49-60, https://doi.org/10.1111/nph.19404, 2024.
- Johnson, M. S., Matthews, E., Bastviken, D., Deemer, B., Du, J., and Genovese, V.: Spatiotemporal Methane Emission From Global Reservoirs, J. Geophys. Res. G: Biogeosci., 126, https://doi.org/10.1029/2021jg006305, 2021.
- Kahl, T., Arnstadt, T., Baber, K., Bässler, C., Bauhus, J., Borken, W., Buscot, F., Floren, A., Heibl, C., Hessenmöller, D., Hofrichter, M., Hoppe, B., Kellner, H., Krüger, D., Linsenmair, K. E., Matzner, E., Otto, P., Purahong, W., Seilwinder, C., Schulze, E.-D., Wende, B., Weisser, W. W., and Gossner, M. M.: Wood decay rates of 13 temperate tree species in relation to wood properties, enzyme activities and organismic diversities, For. Ecol. Manage., 391, 86-95, https://doi.org/10.1016/j.foreco.2017.02.012, 2017.
- Kellner, E., Baird A. J., Oosterwoud M., Harrison K., and Waddington J.M.: Effect of temperature and atmospheric pressure on methane (CH4) ebullition from near-surface peats, Geophys. Res. Lett., 33, https://doi.org/10.1029/2006GL027509, 2006.
 - Kipping, L., Gossner, M. M., Koschorreck, M., Muszynski, S., Maurer, F., Weisser, W. W., Jehmlich, N., and Noll, M.: Emission of CO2 and CH4 From 13 Deadwood Tree Species Is Linked to Tree Species Identity and Management Intensity in Forest and Grassland Habitats, Glob. Biogeochem. Cycles, 36, https://doi.org/10.1029/2021gb007143, 2022.





- Kumar, A. M., Ezhumalai R., Pandey A. K., and S., R. M.: Emission of Methane from Dead Trees / Snags of Tropical and Sub-Tropical Forest Ecoregions, Int. J. Curr. Microbiol. App. Sci., 10, 418-428, https://doi.org/10.20546/ijcmas.2021.1005.049, 2021.
- Liikanen, A., Murtoniemi, T., Tanskanen, H., Vaisanen, T. and Martikainen, P., J.: Effects of temperature and 725 oxygen availability on greenhouse gas and nutrient dynamics in sediment of a eutrophic mid-boreal lake, Biogeochemistry, 59, 269-286, 2002.
 - Linkhorst, A., Hiller, C., DelSontro, T., M. Azevedo, G., Barros, N., Mendonça, R., and Sobek, S.: Comparing methane ebullition variability across space and time in a Brazilian reservoir, Limnol. Oceanogr., 65, 1623-1634, https://doi.org/10.1002/lno.11410, 2020.
- 730 MacPherson, T. A., Cahoon, L. B., and Mallin, M. A.: Water column oxygen demand and sediment oxygen flux: patterns of oxygen depletion in tidal creeks, Hydrobiologia, https://doi.org/10.1007/s10750-007-0643-4, 2007.
 - Martinez, M. and Ardón, M.: Drivers of greenhouse gas emissions from standing dead trees in ghost forests, Biogeochemistry, 154, 471-488, https://doi.org/10.1007/s10533-021-00797-5, 2021.
- 735 Martinez, M., Ardón, M., and Carmichael, M. J.: Identifying Sources and Oxidation of Methane in Standing Dead Freshwater Forested Wetlands, Front. Environ. https://doi.org/10.3389/fenvs.2021.737379, 2022.
 - Megonigal, J. P., Hines, M. E., and Visscher, P. T.: Anaerobic metabolism: linkages to trace gases and aerobic process, Treatise Geochem., 8, 317-424, 2003.
- 740 Oltean L., Teischinger A., and Hansmann C.: Influence of Temperature on Cracking and Mechanical Properties of Wood During Wood Drying - A Review, BioResources, 2, 789-811, 2007.
 - Pangala, S. R., Moore, S., Hornibrook, E. R. C., and Gauci, V.: Trees are major conduits for methane egress from tropical forested wetlands, New Phytol., 197, 524-531, https://doi.org/10.1111/nph.12031, 2013.
- Pangala, S. R., Enrich-Prast, A., Basso, L. S., Peixoto, R. B., Bastviken, D., Hornibrook, E. R. C., Gatti, L. V., 745 Marotta, H., Calazans, L. S. B., Sakuragui, C. M., Bastos, W. R., Malm, O., Gloor, E., Miller, J. B., and Gauci, V.: Large emissions from floodplain trees close the Amazon methane budget, Nature, 552, 230-234, https://doi.org/10.1038/nature24639, 2017.
 - Praetzel, L. S. E., Plenter, N., Schilling, S., Schmiedeskamp, M., Broll, G., and Knorr, K.-H.: Organic matter and sediment properties determine in-lake variability of sediment CO2 and CH4 production and emissions of a small and shallow lake, Biogeosciences, 17, 5057-5078, https://doi.org/10.5194/bg-17-5057-2020, 2020.
 - Reis, P. C. and Barbosa, F. A.: Diurnal sampling reveals significant variation in CO2 emission from a tropical productive lake, Braz. J. Biol., 74, S113-119, https://doi.org/https://doi.org/10.1590/1519-6984.01713,
- 755 Roden, E. E. and Wetzel, R. G.: Kinetics of microbial Fe(III) oxide reduction in freshwater wetland sediments, Limnol. Oceanogr., 47, 198-211, https://doi.org/10.4319/lo.2002.47.1.0198, 2002.
 - Romero-Uribe, H. M., Lopez-Portillo, J., Reverchon, F., and Hernandez, M. E.: Effect of degradation of a black mangrove forest on seasonal greenhouse gas emissions, Environmental Science and Pollution Research, 29, 11951-11965, https://doi.org/10.1007/s11356-021-16597-1, 2022.
- 760 Rosentreter, J. A., Borges, A. V., Deemer, B. R., Holgerson, M. A., Liu, S., Song, C., Melack, J., Raymond, P. A., Duarte, C. M., Allen, G. H., Olefeldt, D., Poulter, B., Battin, T. I., and Eyre, B. D.: Half of global methane emissions come from highly variable aquatic ecosystem sources, Nat. Geosci., 14, 225-230, https://doi.org/10.1038/s41561-021-00715-2, 2021.
- Rosentreter, J. A., Alcott, L., Maavara, T., Sun, X., Zhou, Y., Planavsky, N. J., and Raymond, P. A.: Revisiting 765 Cycle Global Methane Through Expert Opinion, Earth's https://doi.org/10.1029/2023ef004234, 2024.
 - Rudd, J. W. M. and Hamilton, R. D.: Methane cycling in a eutrophic shield lake and its effects on whole lake metabolism, Limnol. Oceanogr., 23, 337-348, https://doi.org/10.4319/lo.1978.23.2.0337, 1978.
- Sakabe, A., Liu, Z., and Kosugi, Y.: Methane Emissions from the Stems of Living and Dead Chamaecyparis 770 obtusa Sieb. Et Zucc, Wetlands, 45, 54, https://doi.org/10.1007/s13157-025-01941-9, 2025.
 - Sanches, L. F., Guenet, B., Marinho, C. C., Barros, N., and de Assis Esteves, F.: Global regulation of methane emission from natural lakes, Scientific Reports, 9, 255, https://doi.org/10.1038/s41598-018-36519-5, 2019
- Saunois, M., Stavert, A. R., Poulter, B., Bousquet, P., Canadell, J. G., Jackson, R. B., Raymond, P. A., 775 Dlugokencky, E. J., Houweling, S., Patra, P. K., Ciais, P., Arora, V. K., Bastviken, D., and Bergamaschi, P., Blake, D. R., Brailsford, G., Bruhwiler, L., Carlson, K. M., Carrol, M., Castaldi, S., Chandra, N., Crevoisier, C., Crill, P. M., Covey, K., Curry, C. L., Etiope, G., Frankenberg, C., Gedney, N., Hegglin, M. I., Höglund-Isaksson, L., Hugelius, G., Ishizawa, M., Ito, A., Janssens-Maenhout, G., Jensen, K. M., Joos, F., Kleinen, T., Krummel, P. B., Langenfelds, R. L., Laruelle, G. G., Liu, L., Machida, T.,
- 780 Maksyutov, S., McDonald, K. C., McNorton, J., Miller, P. A., Melton, J. R., Morino, I., Müller, J.,





810

- Murguia-Flores, F., Naik, V., Niwa, Y., Noce, S., O'Doherty, S., Parker, R. J., Peng, C., Peng, S., Peters, G. P., Prigent, C., Prinn, R., Ramonet, M., Regnier, P., Riley, W. J., Rosentreter, J. A., Segers, A., Simpson, I. J., Shi, H., Smith, S. J., Steele, L. P., Thornton, B. F., Tian, H., Tohjima, Y., Tubiello, F. N., Tsuruta, A., Viovy, N., Voulgarakis, A., Weber, T. S., van Weele, M., van der Werf, G. R., Weiss, R. F., Worthy, D., Wunch, D., Yin, Y., Yoshida, Y., Zhang, W., Zhang, Z., Zhao, Y., Zheng, B., Zhu, Q., Zhu, Q., and Zhuang, Q.: The Global Methane Budget 2000–2017, Earth Syst. Sci. Data, 12, 1561-1623, https://doi.org/10.5194/essd-12-1561-2020, 2020.
- Saunois, M., Martinez, A., Poulter, B., Zhang, Z., Raymond, P. A., Regnier, P., Canadell, J. G., Jackson, R. B., Patra, P. K., Bousquet, P., Ciais, P., Dlugokencky, E. J., Lan, X., and Allen, G. H., Bastviken, D., Beerling, D. J., Belikov, D. A., Blake, D. R., Castaldi, S., Crippa, M., Deemer, B. R., Dennison, F., Etiope, G., Gedney, N., Höglund-Isaksson, L., Holgerson, M. A., Hopcroft, P. O., Hugelius, G., Ito, A., Jain, A. K., Janardanan, R., Johnson, M. S., Kleinen, T., Krummel, P. B., Lauerwald, R., Li, T., Liu, X., McDonald, K. C., Melton, J. R., Mühle, J., Müller, J., Murguia-Flores, F., Niwa, Y., Noce, S., Pan, S., Parker, R. J., Peng, C., Ramonet, M., Riley, W. J., Rocher-Ros, G., Rosentreter, J. A., Sasakawa, M., Segers, A., Smith, S. J., Stanley, E. H., Thanwerdas, J., Tian, H., Tsuruta, A., Tubiello, F. N., Weber, T. S., van der Werf, G. R., Worthy, D. E. J., Xi, Y., Yoshida, Y., Zhang, W., Zheng, B., Zhu, Q., Zhu, Q., and Zhuang, Q.: Global Methane Budget 2000–2020, Earth Syst. Sci. Data, 17, 1873-1958, https://doi.org/10.5194/essd-17-1873-2025, 2025.
- Schmiedeskamp, M., Praetzel, L. S. E., Bastviken, D., and Knorr, K. H.: Whole-lake methane emissions from two temperate shallow lakes with fluctuating water levels: Relevance of spatiotemporal patterns, Limnol. Oceanogr., 66, 2455-2469, https://doi.org/10.1002/lno.11764, 2021.
 - Sherman, B. and Ford, P.: Methane Emissions from Two Reservoirs in a Steep, Sub-Tropical Rainforest Catchment, in: Science Forum and Stakeholder Engagement: Building Linkages, Collaboration and Science Quality, edited by: Begbie D.K., and Wakem, S. L., Brisbane, Queensland, pp 129, 2011.
- Shi, W., Wu, W., Fan, H., Sun, Q., Niu, X., Wang, S., Li, S.-I., Liang, S., and Yan, Z.: Estimating CO₂ and CH₄ fluxes from reservoirs: Model development and site-level study, J. Hydrol., 654, https://doi.org/10.1016/j.jhydrol.2025.132794, 2025.
 - Siegenthaler, A., Welch, B., Pangala, S. R., Peacock, M., and Gauci, V.: Technical Note: Semi-rigid chambers for methane gas flux measurements on tree stems, Biogeosciences, 13, 1197-1207, https://doi.org/10.5194/bg-13-1197-2016, 2016.
 - Sjogersten, S., Siegenthaler, A., Lopez, O. R., Aplin, P., Turner, B., and Gauci, V.: Methane emissions from tree stems in neotropical peatlands, New Phytol., 225, 769-781, https://doi.org/10.1111/nph.16178, 2020.
 - Smart, L. S., Taillie, P. J., Poulter, B., Vukomanovic, J., Singh, K. K., Swenson, J. J., Mitasova, H., Smith, J. W., and Meentemeyer, R. K.: Aboveground carbon loss associated with the spread of ghost forests as sea levels rise, Environ. Res. Lett., 15, https://doi.org/10.1088/1748-9326/aba136, 2020.
 - Tokida, T., Miyazaki T., Mizogucki M, Nagata O., Takakai F., Kagemoto A., and Hatano R.: Falling atmospheric pressure as a trigger for methane ebullition from peatland, Glob. Biogeochem. Cycles, 21, https://doi.org/10.1029/2006GB002790, 2007.
- Tušer, M., Picek, T., Sajdlová, Z., Jůza, T., Muška, M., and Frouzová, J.: Seasonal and Spatial Dynamics of Gas

 820 Ebullition in a Temperate Water-Storage Reservoir, Water Resour. Res., 53, 8266-8276, https://doi.org/10.1002/2017wr020694, 2017.
 - Vroom, R. J. E., van den Berg, M., Pangala, S. R., van der Scheer, O. E., and Sorrell, B. K.: Physiological processes affecting methane transport by wetland vegetation A review, Aquat. Bot., 182, https://doi.org/10.1016/j.aquabot.2022.103547, 2022.
- Walter Anthony K. M. and Anthony, P.: Constraining spatial variability of methane ebullition seeps in thermokarst lakes using point process models, J. Geophys. Res. G: Biogeosci., 118, 1015-1034, https://doi.org/10.1002/jgrg.20087, 2013.
 - Wannikhof, R.: Relationship Bewtween Wind Speed and Gas Exchange Over the Ocean, J. Geophys. Res., 97, 7373-7385, 1992.
- Warner, D. L., Villarreal, S., McWilliams, K., Inamdar, S., and Vargas, R.: Carbon Dioxide and Methane Fluxes From Tree Stems, Coarse Woody Debris, and Soils in an Upland Temperate Forest, Ecosystems, 20, 1205-1216, https://doi.org/10.1007/s10021-016-0106-8, 2017.
 - Whiting, G., J. and Chanton, J., P.: Plant-dependent CH₄ emission in a subarctic Canadian fen, Glob. Biogeochem. Cycles, 6, 225-231, 1992.
- Xun, F., Feng, M., Ma, S., Chen, H., Zhang, W., Mao, Z., Zhou, Y., Xiao, Q., Wu, Q. L., and Xing, P.: Methane ebullition fluxes and temperature sensitivity in a shallow lake, Sci. Total Environ., 912, 169589, https://doi.org/10.1016/j.scitotenv.2023.169589, 2024.
 - Yang, R., Chen, B., Liu, H., Liu, Z., and Yan, H.: Carbon sequestration and decreased CO2 emission caused by terrestrial aquatic photosynthesis: Insights from diel hydrochemical variations in an epikarst spring and

https://doi.org/10.5194/egusphere-2025-5594 Preprint. Discussion started: 19 November 2025 © Author(s) 2025. CC BY 4.0 License.





- two spring-fed ponds in different seasons, Appl. Geochem., 63, 248-260, https://doi.org/10.1016/j.apgeochem.2015.09.009, 2015.
 - Yvon-Durocher, G., Allen, A. P., Bastviken, D., Conrad, R., Gudasz, C., St-Pierre, A., Thanh-Duc, N., and del Giorgio, P. A.: Methane fluxes show consistent temperature dependence across microbial to ecosystem scales, Nature, 507, 488-491, https://doi.org/10.1038/nature13164, 2014.
- Zarfl, C., Lumsdon, A. E., Berlekamp, J., Tydecks, L., and Tockner, K.: A global boom in hydropower dam construction, Aquat. Sci., 77, 161-170, https://doi.org/10.1007/s00027-014-0377-0, 2015.
 - Zhou, Y., Zhang, T., Zhou, L., Zhang, Y., Xu, H., Jang, K. S., Drake, T. W., Grasset, C., Davidson, T. A., Keneally, C. C., Brookes, J. D., and Jeppesen, E.: Terrestrial Organic Matter Inputs Modulate Methane Emissions from a Mega-Reservoir, Environ. Sci. Technol., 59, 6590-6599, https://doi.org/10.1021/acs.est.4c13190, 2025.